

Relating grass failure on the landside slope to wave overtopping induced excess normal stresses

Ponsioen, Luc; van Damme, Myron; Hofland, Bas; Peeters, Patrik

DOI

[10.1016/j.coastaleng.2018.12.009](https://doi.org/10.1016/j.coastaleng.2018.12.009)

Publication date

2019

Document Version

Accepted author manuscript

Published in

Coastal Engineering

Citation (APA)

Ponsioen, L., van Damme, M., Hofland, B., & Peeters, P. (2019). Relating grass failure on the landside slope to wave overtopping induced excess normal stresses. *Coastal Engineering*, 148, 49-56. <https://doi.org/10.1016/j.coastaleng.2018.12.009>

Important note

To cite this publication, please use the final published version (if applicable). Please check the document version above.

Copyright

Other than for strictly personal use, it is not permitted to download, forward or distribute the text or part of it, without the consent of the author(s) and/or copyright holder(s), unless the work is under an open content license such as Creative Commons.

Takedown policy

Please contact us and provide details if you believe this document breaches copyrights. We will remove access to the work immediately and investigate your claim.

Relating grass failure on the landside slope to wave overtopping induced excess normal stresses

Luc Ponsioen

Aveco de Bondt, Podium 9, 3800 GE Amersfoort, The Netherlands

Myron van Damme

Delft University of Technology, Department of Hydraulic Engineering, Stevinweg 1, 2600 GA Delft, The Netherlands

Bas Hofland

Delft University of Technology, Department of Hydraulic Engineering, Stevinweg 1, 2600 GA Delft, The Netherlands

Patrik Peeters

Flanders Hydraulics Research, Flemish Authorities, Berchemlei 115, 2140 Antwerpen Borgerhout, Belgium

Abstract

A high quality safety assessment of levee systems requires a good prediction of when the grass cover of levees fail. Current methods relate the onset of failure to the peak in momentum or energy of the flow, instead of the peak in momentum transfer or energy transfer to the grass cover. The critical velocity necessary in the current methods is thereby difficult to quantify. In line with determining the peak in momentum transfer to the grass, here is shown that the onset of damage of the grass cover can be related to the peak normal stresses acting on the grass cover during wave overtopping. The peak in momentum transfer is thereby assumed to be located at the point of reattachment of the flow with the landside slope. The method is validated against the results of two wave overtopping experiments and benchmarked against the cumulative overload method. An advantage of this method is thereby that both the time and location of the onset of damage can be predicted.

Keywords: Wave Overtopping, Wave Impact Method, Cumulative Overload Method, Grass Failure, Levee

1 Introduction

In line with the new risk based safety assessments performed on levees in The Netherlands and Belgium, the probability of levee failure with respect to applied loads needs to be assessed. An important failure mechanism is erosion of the landside slopes by overtopping waves, as indicated by the 1953 flood of The Netherlands or the effects of Hurricane Katrina in 2004. The most common cover layer of these landside slopes consists of grass on clay. To evaluate the erosion resistance of grass covers on the landside slope of levees, multiple large scale wave overtopping experiments have been performed (Van der Meer et al., 2012). Based on these tests empirical approaches have been developed that relate the damage to grass covers to the local flow velocity, shear stress, or stream power (Dean et al., 2010; Hughes, 2011; Van der Meer et al., 2012).

In this paper, first the main characteristics of the existing empirical approaches for predicting grass failure on landside slopes are discussed. Next, the inferred damage mechanism and the approach for evaluating the impact of the momentum transfer by normal stresses is presented in Section 2. In Section 3, the approach is validated against two field scale wave overtopping experiments. The results are evaluated in Section 4, and conclusions and recommendations are presented in Section 5.

1.1. Damage formation to grass

1.1.1. Existing approaches

Up to a decade ago damage to grass slopes on the landside slopes of levees was mostly related to the mean overtopping discharge (Van der Meer, 2002). Lately, more local hydraulic loads are used to empirically quantify the erosion resistance of grass covers subject to overtopping waves. Dean et al. (2010) used the critical velocity concept for steady overflow from CIRIA 116 (Hewlett, 1985), (Whitehead et al., 1976) to arrive at a relationship for the failure of levees due to overtopping. Dean et al. (2010) thereby related the damage initiation of grass to a mean excess velocity, excess shear stress, or excess stream power. The excess stream power showed the smallest errors and was therefore the recommended method of damage description. Van der Meer et al. (2012) extended the approach by Dean et al. (2010). Instead of using mean values for the shear stress or stream power, Van der Meer et al. (2012) hypothesized that peak loads during wave overtopping are likely to contribute significantly more to the onset of damage than mean loads. This led to the cumulative overload method. For a certain location on the grass cover, the cumulative overload method predicts a damage factor D from (Van der Meer et al.,

37 2012).

$$D_{CO} = \sum_{i=1}^{i=n} (a_p u_p^2 - u_c^2) \quad (1)$$

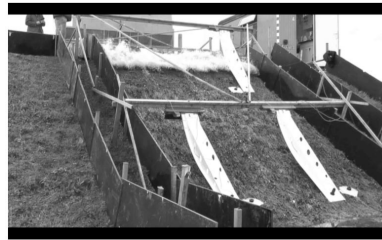
38 where u_c is the critical velocity [m/s] and u_p is the peak velocity [m/s] that follows
39 empirically from (Van der Meer et al., 2012):

$$u_p = 4.5V^{0.3} \quad (2)$$

40 With V the wave overtopping volume [m²] and a_p is a flow acceleration factor
41 which will be larger than 1, increasing down the slope. According to Van der Meer
42 et al. (2012) initial damage is expected when $D_{CO} = 500$, severe damage should be
43 observed when $D_{CO} = 1000$ and complete failure occurs when $D_{CO} = 3500$. These
44 values are prone to large scatter.

45 Characteristic of these approaches (Dean et al., 2010; Hughes, 2011; Van der
46 Meer et al., 2012) is that damage is assumed to initiate when a velocity, shear
47 stress, or stream power exceeds a critical value. The summation of the excess
48 load is an indicator of the extent of the damage induced by overtopping waves.
49 The cumulative overload method by Van der Meer et al. (2012) is stress based and
50 consequently related to u^2 , whereas the mean excess load approach (Dean et al.,
51 2010; Hughes, 2011) is energy based and uses u^3 . As the flow velocity increases
52 along the landside slope, due to acceleration of the flow by gravity, damage is
53 consequently most likely to initiate at the toe of the landside slope.

54 A close evaluation of the excess velocity, stress, or stream power (Dean et al.,
55 2010; Hughes, 2011) or cumulative overload (Van der Meer et al., 2012) have high-
56 lighted two problems. First, critical velocity values required for these methods are
57 difficult to quantify. During steady overflow tests performed on grass (van Damme
58 et al., 2016; Cantré et al., 2017) it was noted that the critical velocity needed to
59 initiate damage to the grass far exceed predictions given by Hewlett (1985) and
60 Whitehead et al. (1976). Second, according to the excess stress or excess volume
61 approach grass covers should predominantly fail near the bottom of the landside
62 slope as the energy of the flow is maximum there due to the acceleration of the
63 flow along the landside slope. However grass has also been observed to fail near the
64 top of the landside slope. Below the second knowledge gap is addressed, whether
65 damage initiation should be correlated only with the slope parallel flow velocity,
66 or (also) with the peak in momentum transfer perpendicular to the levee. This is
67 done by relating damage to the normal stresses exerted on the grass by overtopping
68 waves.



(a) Overtopping at the crest



(b) Separation from the landside slope



(c) Close to reattachment with landside slope



(d) Point of impact

Figure 1: Wave separation from the bed and an impact during a $2 \text{ m}^3/\text{m}$ overtopping wave volume. Observed during wave overtopping tests at Wijmeers, Belgium.

69 *1.1.2. Proposed approach*

70 During wave overtopping experiments performed at Wijmeers (van Damme
71 et al., 2016) it was noted that overtopping waves separated at the end of the crest
72 before reattaching with the landside slope, as can be seen in Figure 1. The impact
73 of an overtopping wave was more powerful and the impact zone was further down
74 the landside slope than the impact of overtopping flow due to a higher flow velocity
75 at the crest. It was inferred that at the point of reattachment both shear stresses and
76 normal stresses are transferred to the levee surface. The significant normal stress
77 component at the point of reattachment of overtopping waves causes for a peak
78 in momentum transfer higher up the landside slope. Differences in normal stresses
79 exerted on the landside slope of the levee between overflow and overtopping would
80 explain why grass covers fail during overtopping but not during overflow. Here the
81 hypothesis is tested whether the location of damage on the landside slope due to
82 wave overtopping could be caused by peaks in momentum transfer due to the normal
83 impact by overtopping waves.

84 The envisaged damage mechanism by which the grass cover fails is depicted in Fig-
85 ure 2. Grass failure is expected to start with existing small cracks in the grass/clay
86 cover (See Figure 2a). These cracks are often present due to natural expansion

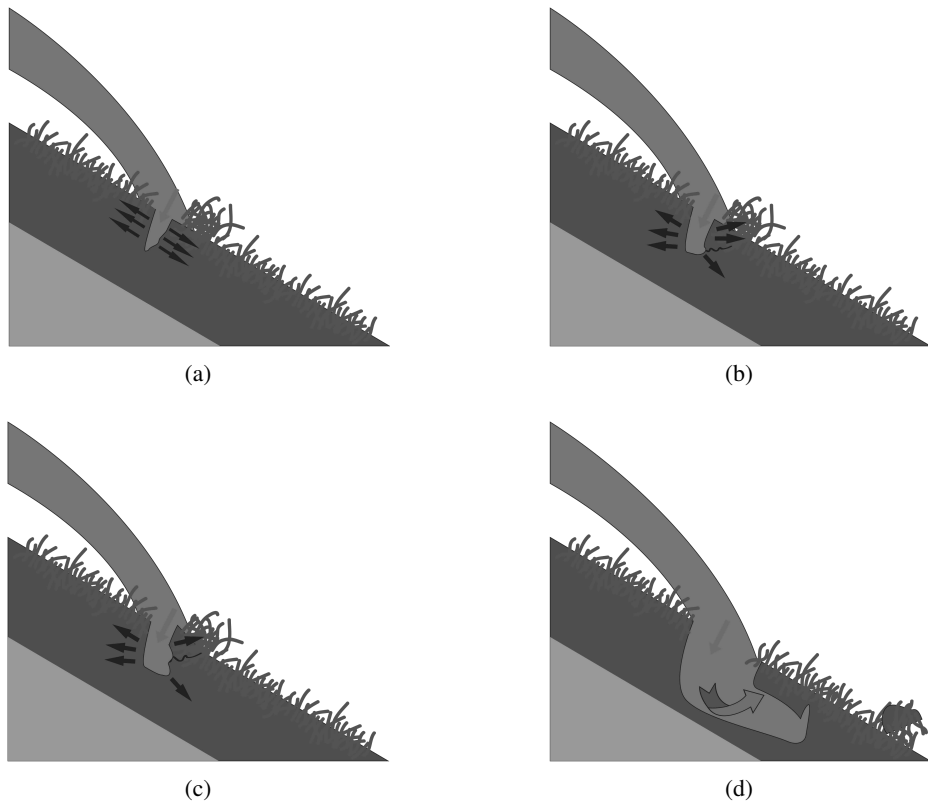


Figure 2: Failure initiation process observed during the overtopping experiment at Wijmeers

87 and shrinkage of the clay cover. Normal forces exerted on the landside slope by
88 overtopping waves (Figure 2b) cause these cracks to widen. In accordance with
89 Führböter (1966), the increase in water pressure in the crack during wave impact
90 is expected to push the walls of the crack aside and cause for the crack to deepen.
91 When the crack extends over the depth of the turf layer, grass can reasonably be
92 expected to become subject to deformation due to lower cohesion of the clay un-
93 der the turf layer compared to that of the root/clay mixture (Figure 2c). The hole
94 that originates under the grass cover will then cause for the grass aggregate to be
95 pushed up (Figure 2d), allowing for further expansion of the hole under the grass
96 by flow induced scour. The continuous increase of space beneath the grass, causes
97 grass aggregates to be pushed out of the soil. The flow over the grass cover and
98 the overpressure under the grass cover separates the grass sod from the clay layer,
99 making it roll up like a carpet in downstream direction, which is in accordance with
100 observations made by Hai and Verhagen (2014). At a certain moment the induced
101 pressure under the grass cover becomes too high leading to a piece of grass sod to
102 be ripped from the grass cover and washed away by the flow.

103 Depending on the curvature of the levee at the intersection of the crest and
104 landside slope overtopping waves separate from the landside slope at the down-
105 stream end of the crest before reattaching with the landside slope further down the
106 landside slope (see Figure 1). The point of reattachment of large volume waves is
107 thereby located further downstream than for small volume waves. This is due to the
108 higher horizontal flow velocity component at the downstream end of the crest. This
109 process was observed during the Wijmeers overtopping experiments (van Damme
110 et al., 2016) whereby immediate failure of the grass cover initiated after one 3000
111 l per m wave. The hypothesis that the location of grass failure is related to the
112 summation of normal stresses exerted by overtopping waves to the slope at the
113 location of reattachment is furthermore supported by reports on the overtopping
114 experiments in Zeeland (Bakker et al., 2008). Here damage to the grass cover first
115 initiated at the end of the landside slope where the flow was redirected and hence a
116 significant momentum was exchanged with the grass cover. Based on this hypoth-
117 esis a new approach was developed which relates the initiation of damage to the
118 normal stresses at the point of reattachment. Hereonwards this approach is referred
119 to as the wave impact approach.

120 **2. Wave impact approach**

121 *2.1. Normal stresses acting on the grass cover*

122 To evaluate the normal stresses exerted on the levee the location of wave im-
123 pact is determined and compared to the location of the (initial) damage. In a Carte-
124 sian reference framework, the horizontal distance traveled by a wave is given by

125 $X(t) = u_x(t) \cdot t$, where $X(t)$ is the horizontal, time dependent, coordinate of
 126 reattachment relative to the intersection of the crest and landside slope, $u_x(t)$ is
 127 the horizontal velocity component, t [s] is the separation time. During the separa-
 128 tion time, the wave is curved downwards under influence of gravity. The vertical
 129 distance travelled is thereby given by $Z(t) = -\frac{1}{2}gt^2$, where $Z(t)$ is the relative
 130 vertical distance travelled, and g is the gravitational constant.

131 Here the flow characteristics are obtained from the following approximation
 132 provided by Hughes et al. (2012). The peak discharge q_p [m^2/s] at the end of the
 133 crest has been related to the overtopping wave volume V [m^2] via (Hughes et al.,
 134 2012)

$$q_p = 0.184\sqrt{g}V^{\frac{3}{4}} \quad (3)$$

135 T_0 is the overtopping duration which can be derived from the wave volume accord-
 136 ing to (Hughes et al., 2012) (with dimensions for q_p , V , and T_0 , respectively m^2/s ,
 137 m^2 , and s).

$$T_0 = \frac{V^{1.16}}{0.43q_p} \quad (4)$$

Under the assumption that d_p and u_p appear at the same location (Hughes, 2011),
 the reduction in depth and velocity over time are given by

$$u_{\text{crest}}(t) = u_p \left(1 - \frac{t}{T_0}\right)^a \quad (5)$$

$$d_{\text{crest}}(t) = d_p \left(1 - \frac{t}{T_0}\right)^b \quad (6)$$

138 Here a and b are parameters which determine the matter of decrease in velocity or
 139 water depth with time. Often this decrease is assumed to be linear, therefore both
 140 a and b are assumed to be 1. The peak depth d_p [m] could be related to the peak
 141 discharge according to (Hughes et al., 2012)

$$q_p = \left(\frac{2}{3}\right)^{\frac{3}{2}} \sqrt{g} d_p^{\frac{3}{2}} \quad (7)$$

142 Assuming d_p and u_p appear at the same location, the peak velocity u_p is determined
 143 by

$$u_p = \frac{q_p}{d_p} \quad (8)$$

144 Assuming a uniform velocity distribution over the water depth at the down-
 145 stream side of the crest, the extents of the wave impact area per unit width have
 146 now been determined by a new approach named the Wave Impact approach. The
 147 area of impact is thereby assumed to equal the flow area at the end of the landside

148 slope. Any errors in mass balance have thereby been assumed negligible. The ex-
 149 tents of the impact zone are defined by $X_{\text{wave,min}}(t)$, $Z_{\text{wave,min}}(t)$ and $X_{\text{wave,max}}(t)$,
 150 $Z_{\text{wave,max}}(t)$. The horizontal velocity component at the location of impact is as-
 151 sumed to be identical to the horizontal velocity component at the downstream end
 152 of the crest (see Equation 5) which leads to

$$Z_{\text{wave,min}}(t) = -\frac{1}{2}g \left(\frac{X_{\text{wave,min}}(t)}{u_{\text{crest}}(t)} \right)^2 = -X_{\text{wave,min}}(t)\tan \theta \quad (9)$$

153 where θ is the slope angle of the landside slope, and

$$X_{\text{wave,min}}(t) = \frac{2 \cdot u_{\text{crest}}^2(t)\tan \theta}{g} \quad (10)$$

154 Equations 9 and 10 could be written for the maximum impact coordinates by
 155 replacing $X_{\text{wave,min}}(t)$ and $Z_{\text{wave,min}}(t)$ for $X_{\text{wave,max}}(t)$ and $Z_{\text{wave,max}}(t)$. The ver-
 156 tical velocity component at the point of impact follows from

$$u_z(t) = \sqrt{2gZ_{\text{wave}}(t)} \quad (11)$$

157 The maximum location of impact is defined in a similar way as the minimum
 158 impact coordinate, with addition of the flow depth at the crest. The maximum
 159 impact coordinate is assumed to be determined by the top of the stream at the crest.
 160 When the streamline of the top of the flow is tracked, the maximum impact location
 161 is found. When d_{crest} is the flow depth at the crest, the maximum impact location
 162 is determined by

$$X_{\text{wave,max}}(t) = \frac{u_{\text{crest}}^2(t)}{g} \left(\tan \theta + \sqrt{\tan^2 \theta + \frac{2gd_{\text{crest}}(t)}{u_{\text{crest}}^2(t)}} \right) \quad (12)$$

163 whereby u_{crest} and d_{crest} are obtained from Equations 5 and 6. With u_x and u_z
 164 known in the Cartesian coordinate system, the velocities can also be obtained in
 165 the $\hat{\chi}, \hat{\zeta}$ coordinate system whereby the $\hat{\chi}$ coordinate direction is parallel to the
 166 landside slope and the $\hat{\zeta}$ coordinate direction is perpendicular to the landside slope.
 167 θ is the angle with which the coordinate system rotates which is here equal to the
 168 landside slope angle. When the angle of impact of the overtopping wave on the
 169 landside slope is determined by β , the stress delivered to the landside slope due to
 170 the normal impact is now given by

$$\sigma_{\zeta\zeta} = \rho u_{\zeta} |u_{\text{imp}}| \sin \beta = \rho (u \sin \theta + \omega \cos \theta) \sqrt{u^2 + \omega^2} \sin \beta \quad (13)$$

171 where u_{imp} is the impact velocity. The wave impact induces a pressure on the grass
 172 cover which is assumed to be related to the location and initiation of failure of the

173 grass cover. It should be noted that Equation 13 describes the pressure which is
 174 exerted on a slope under steady state flow conditions. The actual normal force at
 175 the initial impulsive impact may be different. However, for a first assessment of
 176 the validity of the wave impact approach the steady state pressure approximation
 was deemed sufficient. This is demonstrated in Figure 3.

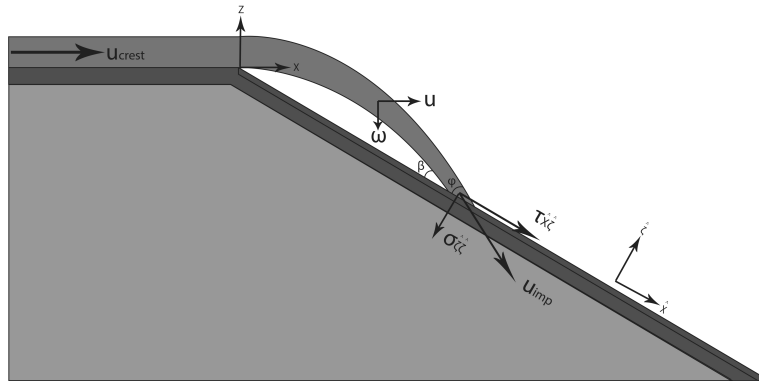


Figure 3: Normal stress per unit width approach

177
 178 During an overtopping event the discharge, depth, and flow velocity of a wave
 179 decrease. The location of impact thereby retreats along the landside slope towards
 the crest. This phenomenon is demonstrated in Figure 4. The location and initi-

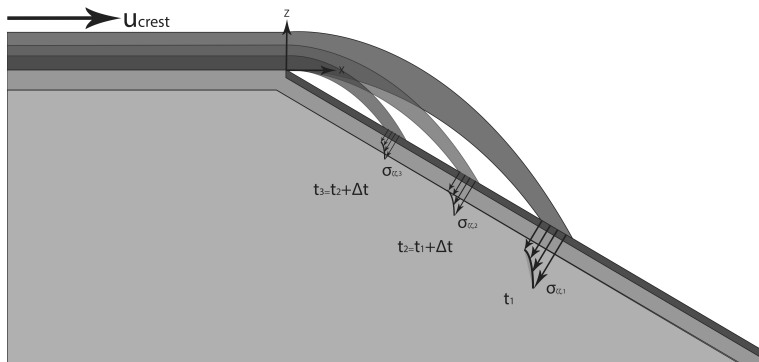


Figure 4: Changes in impact location during a single overtopping event

180
 181 ation of grass failure are assumed to be related to the total transfer of momentum
 182 J_{ζ} which is given by the normal stress multiplied by duration. During a single
 183 wave overtopping event the area of wave impact is retreating in upstream direc-
 184 tion. Hence, per overtopping event the net area affected by one wave is larger than
 185 the initial area of impact but encompasses the area upstream of the initial impact

186 area. A small normal stress applied for a longer time thereby can produce a similar
 187 transfer of momentum (the same impulse) as a large stress applied briefly. Hence
 188 the location of damage initiation does not have to coincide with the area of impact
 189 of the largest waves. Supplementary to this phenomenon, the top of the wave reat-
 190 taches slightly further down the landside slope than the bottom of the wave. As the
 191 overtopping discharge and velocity decrease, the top of the wave retreats over the
 192 initial points of impact on the slope of the bottom of the wave.

193 To determine the exchange of momentum to a specific location on the landside
 194 slope, each overtopping induced stress event at location X is integrated over time.
 195 When multiple waves overtop the levee and reattach on the landside slope, the
 196 total transferred momentum at location X is determined by the summation of the
 197 integrals of all overtopping waves. This is given by

$$J_{\zeta}(X) = \sum_{n=1}^N \int_t^T \sigma_{\zeta\zeta,n}(X, t) dt \quad (14)$$

198 where $\sigma_{\zeta\zeta,n}$ is a function of location X and time t . N is the amount of overtop-
 199 ping wave events and T is the duration over which the momentum is transferred at
 200 location X . $\sigma_{\zeta\zeta,n}(X, t)$ in Equation 14 is written in terms of horizontal land side
 201 slope coordinate $X(t)$ and flow velocity at the crest u_{crest} according to

$$\sigma_{\zeta\zeta}(t) = \rho(u_{\text{crest}}^2(t) + 2gX(t) \tan \theta) \cdot \sin \beta \quad (15)$$

202 For $X(t)$ see Equation 12. Damage initiates when the stresses induced on the
 203 landside slope exceeds a critical pressure. In order to evaluate whether the forces
 204 acting on the grass cover are significant to initiate damage, the resistance of the
 205 grass cover has been evaluated below.

206 2.2. Resistance of the grass cover to normal stresses

207 Stanczak (2007, 2008) and Führböter (1966) hypothesized for plunging waves
 208 connecting with a grass cover on the waterside slope that the wave impact pres-
 209 sure induces two horizontal forces. Based on an undrained failure of clay Stanczak
 210 (2007, 2008) and Führböter (1966) stated that a crack forms or widens when the
 211 impact pressure exceeds the threshold pressure P_c denoted by twice the cohesion
 212 of the clay layer. Richwien (2003) extended the approach of Führböter (1966) by
 213 including other parameters such as the weight of the soil body G , the reaction of
 214 the soil Q and the pore water pressure U based on a simplified, graphical analy-
 215 sis of forces. Stanczak (Stanczak, 2008, 2007), criticized the theories developed
 216 by Führböter (1966) and Richwien (2003) as they assume an idealized situation.
 217 Stanczak however did also admit that application of more advanced models is chal-
 218 lenging. Here the theory developed for the impact of plunging waves on waterside

219 slopes by Führböter (1966) has been applied to the case of overtopping waves im-
 220 pacting on the landside slope. The threshold pressure P_c , required to enlarge cracks
 221 in the grass cover, is given by the strength of clay and grass combined. Figure 2
 222 demonstrates how pressures in excess of the critical pressure cause the walls of a
 223 crack to be pushed aside. The critical pressure of twice the cohesion (Führböter,
 224 1966) corresponds well with the theoretical threshold stress level of cutting clay
 225 underwater as done during dredging (Miedema, 2014). However cutting tests per-
 226 formed with steel blades on clay indicate that the critical pressure P_c is a function
 227 of several factors like the geometry and loading situation. In general the critical
 228 pressure level is expected to vary between $2c' \leq P_c \leq 5c'$ (Van der Schrieck,
 229 2006). A value of $5c'$ also corresponds with the artificial root cohesion found by
 230 Hoffmans (2014). It should thereby be noted that the effects of artificial cohesion
 231 by capillary action are not accounted for. The characteristic value of c' is there-
 232 fore likely to be conservative. However the value may correspond with the degree
 233 of cohesion of weaker spots on the landside slope. In the remained of this paper
 234 has been assumed that the critical pressure required to initiate damage is given by
 235 $2c' \leq P_c \leq 5c'$. Damage to the grass cover is initiated when the wave impact in-
 236 duced normal stress delivered to the landside slope $\sigma_{\zeta\zeta}$ exceeds the critical pressure
 237 P_c .

238 The location of failure is assumed to coincide with the location where the total
 239 excess momentum transferred J_E is maximum. This location now follows from

$$J_E = \sum_{n=1}^N \int_t^T (\sigma_{\zeta\zeta,n}(X, t) - P_c) dt \quad (16)$$

240 Equation 16 highlights the main benefit of the wave-impact approach over the ex-
 241 cess volume approach, namely that it is possible to validate the wave impact ap-
 242 proach based on the location of failure, as well as the moment of initiating failure.
 243 Below, the wave impact approach has been tested and bench-marked against the
 244 excess volume approach of Van der Meer et al. (2012).

245 3. Testing of the wave impact approach

246 The assumption that the failure of grass is related to the sum of normal stresses
 247 exerted on a slope during wave overtopping has been tested against the results of
 248 two wave overtopping experiments. The first experiment was the experiment per-
 249 formed at Wijmeers (van Damme et al., 2016) and the second was the overtopping
 250 experiments performed in Zeeland (Bakker et al., 2008). For those overtopping
 251 tests where damage on the landside slope occurred a value for the critical stress
 252 P_c was determined based on prior performed overtopping tests on the same test

253 section at a lower mean overtopping discharge. After setting the value for P_c the
254 results were compared against the location of damage that was observed during the
255 wave overtopping tests to evaluate how well the peak momentum transferred coin-
256 cided with the location of initial damage on the landside slope. The found value of
257 P_c was then compared with the theoretical value.

258 For the Wijmeers experiment, the wave overtopping volumes that had been
259 released on the levee were obtained from the testing script. For the experiments
260 in Zeeland, the exact overtopping volumes were recreated assuming Weibull dis-
261 tributed wave overtopping volumes. The shape and scale parameters for the Weibull
262 distribution were obtained from the test description and the EurOtop manual (Eu-
263 rOtop, 2007). Based on the overtopping volumes the peak discharge was derived
264 from Equation 3. The peak depth and peak velocity at the end of the crest were
265 derived from respectively Equations 7 and 8, and the overtopping time was ob-
266 tained from Equation 4. The velocity at the end of the crest was assumed to reduce
267 linearly with time (see Equation 15) and uniformly distributed over the depth. The
268 depth was divided in 10 equal sized slices. For each time step of 0.01 s the location
269 of impact and corresponding normal stress has been assessed. The landside slope
270 has been subdivided into a grid of 0.10 m wide. The momentum transferred in each
271 grid cell has been added up to arrive at a distribution of total momentum transfer
272 along the landside slope.

273 3.1. Wijmeers

274 During the Wijmeers experiment two dike sections were subjected to wave
275 overtopping tests and 2 sections to overflow tests. During the overflow tests it
276 became apparent that the grass cover was able to withstand mean overflow dis-
277 charges of 170 l/s per m whereby the flow velocities were in excess of 3.5 m/s
278 (van Damme et al., 2016). During the overtopping tests the first 4 m wide test
279 section was subjected to wave overtopping volumes of respectively 1, 5, 10, 25 l/s
280 and 50 l/s per m. The second 4 m wide test section was subjected to waves of 25
281 l/s per m after the hydraulic measurements had been performed on this section. A
282 full test description is provided by (van Damme et al., 2016). The wave conditions
283 underlying the test programme are provided in Table 1. In Table 1 V_p denotes the
284 maximum overtopping volume, N_{ot} the number of overtopping waves, P_{ot} the over-
285 topping probability, T_p [s] the peak wave period, H_s the significant wave height,
286 and q the mean overtopping discharge.

287 During the first overtopping experiment the crest line was located 3 m from the
288 outflow opening of the simulator. Along the slope at a distance of approximately
289 1 m the surface of the slope had clearly dropped, however the grass cover was still
290 intact. The corresponding critical stress for the grass cover at Wijmeers was there-
291 fore calibrated at $P_c = 10 \text{ kN/m}^2$, which corresponds with a situation whereby no

Table 1: Overtopping parameters Wijmeers.

q [l/s/m]	1	5	10	25	50
H_s [m]	0.4	0.6	0.8	1.2	1.3
T_p [s]	2.53	3.10	3.58	4.38	4.56
P_{ot}	0.181	0.336	0.386	0.449	0.575
N_{ot}	617	936	931	858	1089
V_p [l/m]	113	349	672	1662	2230

292 damage at all would occur to the grass cover during a 5 l/s per m test. It should
 293 however be noted that at a distance of 1m along the landside slope already some
 294 settlement occurred during the 5 l/s per m test. However this settlement was ini-
 295 tiated by a locally present rabbit hole and was not believed to be due to the forces
 296 exposed on the grass cover by the overtopping waves. A damage occurring around
 297 the 1 m line corresponds with a horizontal distance of $X = 0.85m$. Applying this
 298 critical stress value to Equation 16 gives the distribution of transferred momentum
 299 along the Cartesian x -axis shown in the top graph in Figure 5. As the second test
 300 section was located close to the first test section, the same value for the critical
 301 pressure was applied. On this second test section first hydraulic measurements
 302 were performed with wave volumes of 500 l/m increasing incrementally at steps
 303 of 500 l/m to waves of 3500 l/m. With the exception of the 3000 and 3500 l/m
 304 waves every wave volume had been released three times in concession. The larger
 305 waves already damaged the top layer of the grass cover although the root system
 306 was still in place. The damage was predominantly focused on the lower half of the
 307 landside slope. During the 25 l/s per m test, damage progressed predominantly at
 308 a horizontal distance of $1.3 \leq X \leq 2.15$ m from the landside end of the crest. The
 309 distribution of momentum exchange for this experiment is given in Figure 5b.

310 In Figure 5b 2 lines have been presented. The line with $P_c = 10$ kN/m² is
 311 based on the assumption that no damage is allowed to occur for the 1 and 5 l/s
 312 per m experiments. The second line is calibrated against the observed location of
 313 damage during Experiment 1. During the first overtopping experiment the grass
 314 cover failed at the location of a rabbit hole just beneath the surface. For a slightly
 315 sandy clay subsoil the estimated value of cohesion c' is 5 kN/m². The more sand
 316 is present the lower the expected value of the cohesion is. The value of P_c whereby
 317 damage initiates therefore corresponds with a value of $P_c = 2c'$.

318 For comparison the cumulative overload method has been applied to the re-
 319 sults of the Wijmeers experiment in eq.(2). Figure 5c shows the damage factor as
 320 a function of the critical velocity for each of the tests performed at Wijmeers. The
 321 damage factor for severe damage ($D = 1000$) is represented in 5c with a horizontal

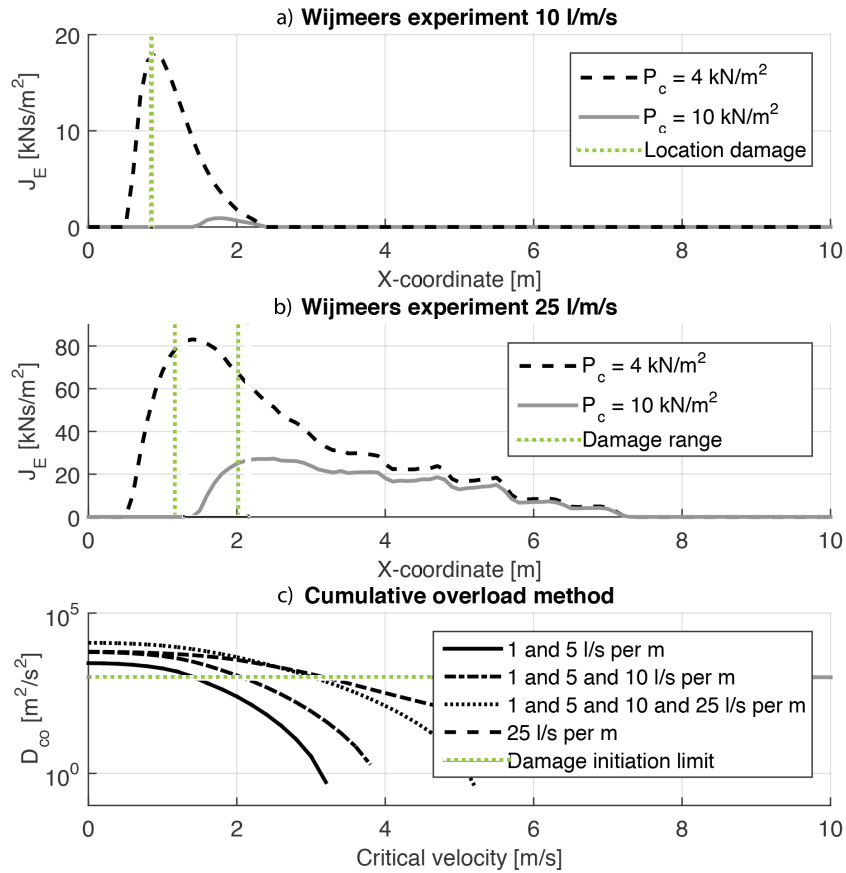


Figure 5: Distributions of excess momentum transferred to the landside slope during the overtopping experiments at Wijmeers (figure *a* and *b*), two curves are presented; a) dotted line with $P_c = 4 \text{ kN/m}^2$ refers to the rabbit hole and b) $P_c = 10 \text{ kN/m}^2$ refers to the highest critical pressure at which damage could be expected. The results of the cumulative overload method when applied to Wijmeers are presented in figure *c*.

322 line. At Wijmeers damage started during the 10 l/s per m overtopping test and sig-
 323 nificantly grew during the 25 l/s per m overtopping experiment. This corresponds
 324 with a critical velocity value of 2 m/s, which in turn corresponds with the critical
 325 velocity that follows from the grass resistance curves given in the Technical Note
 326 71 (Whitehead et al., 1976). However during overflow tests, it was noted that grass
 327 was able to withstand flow velocities in excess of 3.5 m/s. This difference in crit-
 328 ical velocity may highlight that the methods by Hughes (2011), Dean et al. (2010)
 329 and Van der Meer et al. (2012) might need some modification as the Wijmeers
 330 experiments indicate that the theoretical critical velocities do not well match the
 331 observed critical velocities.

332 3.2. St. Philipsland overtopping experiments

333 The tested landside slope at the St. Philipsland dike was 13 m long with a
 334 1 : 2.4 slope, or a slope angle $\theta = 0.39$ rad. The grass cover was in good con-
 335 ditions according to the VTV2006 standards. Below the grass cover a clay layer
 336 of approximately 0.40m thickness was present. For a good quality clean clay the
 337 expected undrained cohesion values are according to Table 2b of the NEN 1997:
 338 $c' = 13 - 15 \text{ kN/m}^2$. The wave overtopping conditions to which the levee was
 exposed are given in Table 2

Table 2: Overtopping conditions to which the levee at St. Philipsland was exposed, for $H_s = 2\text{m}$ and $T_m = 4.7\text{s}$, and a storm duration of 2 hours

q [l/s/m]	0.1	1	10	30	50	75
P_{ot}	0.002	0.027	0.189	0.366	0.47	0.56
N_{ot}	3	42	289	561	720	858
V_p [l/m]	400	858	2110	3790	5180	6750

339 During the overtopping experiments at St. Philipsland initial damage spots
 340 were noticed around the respectively 4 and 7 m line below the crest line. At the
 341 4 m line, which corresponds to $X = 3.7$ m, a minor bold spot was visible in the
 342 grass cover. At the 7 m line, which corresponds to $X = 6.5$ m, a minor headcut
 343 had formed. The initial damage spot around the 7 m line eventually developed into
 344 a big eroded area just above the toe.
 345

346 The damage predictions for St. Philipsland experiment show two lines (See
 347 Figure 6). In the second graph the first line corresponds with $P_c = 22 \text{ kN/m}^2$
 348 which has been calibrated for the case whereby no damage occurred during the
 349 1, 10, and 30 l/s per m test. The second line corresponds with $P_c = 33 \text{ kN/m}^2$
 350 which corresponds with the situation whereby no damage occurs during the 1, 10, 30,
 351 and 50 l/s per m tests. During the 30 l/s per m test some damage to the grass cover
 352 initiated at the connection with the boards bordering the side of the test section.

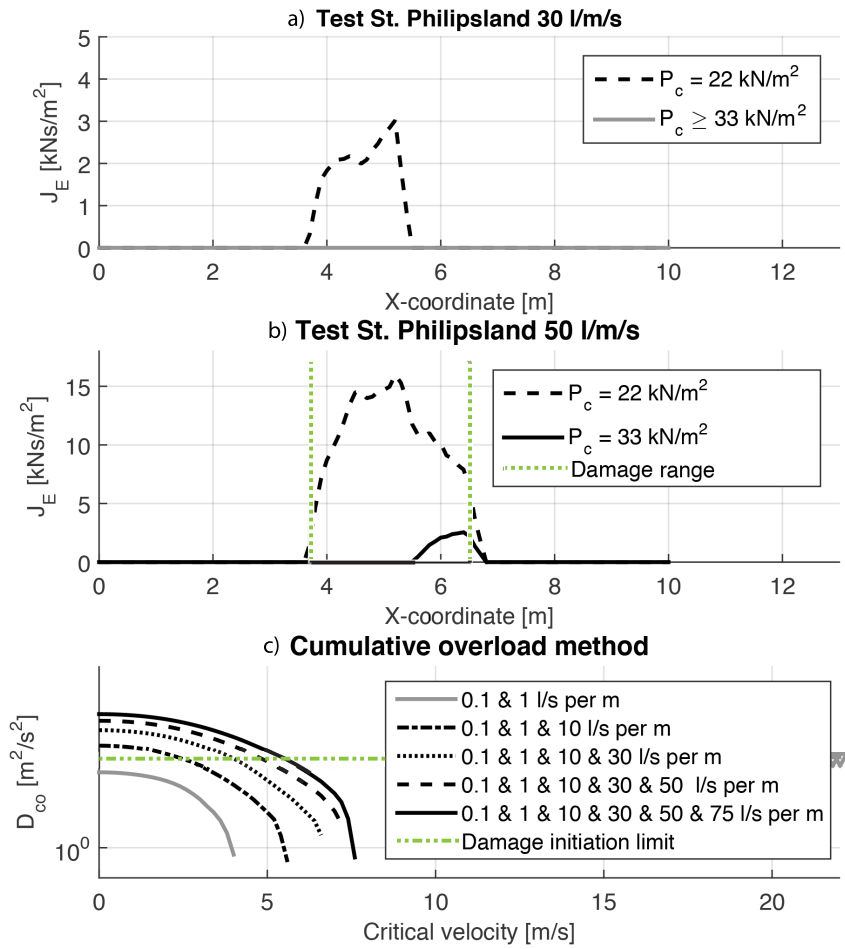


Figure 6: Distribution of excess momentum transferred to the landside slope if no failure occurred during for the 10 l/s per m experiment at St. Philipsland

353 During the 50 l/s per m test however the damage initiated on the test section itself
354 at the 6m and 9 m distance from the outflow opening of the wave impact simula-
355 tor. The slope started at 2 m distance from the outflow opening of the simulator.
356 Hence, for a slope of 1 : 2.5 the locations of the damage correspond with re-
357 spectively $X = 3.7\text{m}$ and $X = 6.5\text{m}$. These predictions are a close match with
358 the actual location where damage initiated. The values of $P_c = 22 \text{ kN/m}^2$ and
359 $P_c = 33 \text{ kN/m}^2$ correspond with values for the cohesion of $c' = 7.3 \text{ kN/m}^2$ and
360 $P_c = 11 \text{ kN/m}^2$. Here the value of $P_c = 33 \text{ kN/m}^2$ gives a better correspondance
361 with the location of grass failure, and expected value for the cohesion.

362 4. Discussion

363 Evaluating the predictions of the wave impact approach has highlighted some
364 interesting aspects. First the locations where the grass failures initiated were all
365 subject to normal stresses indicating that a peak in momentum transfer may better
366 describe the initiation of grass failure than a peak in stream power of the flow. At
367 the test site at Wijmeers a clay layer was present at the landside slope which was
368 protected by a poor quality grass cover. The grass cover failed during the first test
369 at the location of a rabbit hole beneath the surface. The location of this rabbit hole
370 is likely to have negatively influenced the resistance of the levee against overtop-
371 ping. For a cohesive value of 4 kN/m^2 however a good match is found between
372 the peak excess momentum transfer and the location of damage during both the
373 first and the second wave overtopping experiment. When applying the cumulative
374 overload method to the Wijmeers experiment then one finds a critical velocity of
375 2 m/s . During the overflow experiments that were performed at Wijmeers it how-
376 ever became apparent that the grass cover was able to withstand flow velocities
377 in excess of 3.5 m/s for up to 6 hours. The difference in flow velocity could be
378 partially attributed to a difference in shear stress. However, in this case a critical
379 stress may be a better parameter to use than a critical velocity value because stress
380 could be directly related to the wave impact induced pressure. In some cases also
381 an acceleration factor is applied to the cumulative overload method to account for
382 the increase in velocity between the downstream end of the crest and the location
383 where the damage occurred. In the case of Wijmeers however, damage initiated
384 near the downstream end of the crest. It is therefore expected that the influence of
385 the acceleration factor alone will not be able to explain the observed differences in
386 critical velocity between the overtopping and overflow experiments. A clear differ-
387 ence between loading due to overflow and wave overtopping is that wave impacts
388 induce significantly higher normal stresses on the levee at the point of reattach-
389 ment than overflow. A normal stress based approach like the Wave Impact method
390 is therefore able to explain why damage would occur during wave overtopping and
391 not during overflow. The discrepancies found in the calibrated critical velocities
392 and the resistance against the applied overflow velocities indicates that equations
393 that apply a critical velocity parameter are not able to explain why a landside slope
394 grass cover fails during wave overtopping but is able to withstand an overflow. The
395 Wave Impact method is also able to indicate those locations along the landside
396 slope where the highest wave overtopping induced load could be expected during
397 a storm. The method indicates when damage is to be expected (i.e. $J_E > 0$ means
398 damage) but it is limited in predicting the amount of damage caused by the over-
399 topping waves, therefore, further research on the value of the magnitude of the
400 excess momentum J_E is recommended. When a certain critical load indicator (for

401 instance $J_{E,c}$) could be defined, indicating when the grass cover is classified as
402 'failed', the Wave Impact method predicts the wave overtopping induced landside
403 slope damage more accurately.

404 For the St Philipsland case the wave impact method was able to accurately pre-
405 dict the location where damage would initiate after calibrating the critical pressure
406 based on the tests during which no failure occurred. Due to the sole dependence
407 of the damage coefficient in cumulative overload method on the critical velocity
408 always one critical velocity value can be found for which the cumulative overload
409 method accurately hind-casts at what moment damage initiated.

410 Estimates of the critical pressure were found to correspond well to the expected
411 range of $P_c = 2 - 5c'$ whereby c' is the characteristic value for the undrained co-
412hesion. It should be noted that for validation purposes the critical pressure and the
413 critical velocity have been kept constant per dike section. The wave impact method
414 thereby works with the assumption that the horizontal velocity of the wave does not
415 change after it separates from the embankment. It is recommended to further study
416 the validity of this assumption by measuring the location where the wave impacts
417 on the landside slope. It is thereby recommended to also measure the impact pres-
418sures on the landside slope to identify whether these are significant enough to lead
419 to failure of the grass cover. In the wave impact method the location of failure was
420 related to the peak normal stresses that occurred. This hypothesis is strengthened
421 by the observations of damage that occurred where the landside slope gradient of
422 a levee reduces, for example due to a berm structure. In the cumulative overload
423 method (Van der Meer et al., 2012) the shear stress is assumed to determine the
424 moment of failure. It is recommended to further study which loading mechanism
425 is dominant or whether grass failure is best described by a combination of these
426 two loading mechanisms. For example, failure could be related to the total stress
427 instead of just the normal stress component. The difference in the predicted critical
428 velocities and the velocities obtained during the overflow tests during the Wijmeers
429 experiments, and the high critical flow velocities does indicate occurrence of an-
430 other initiation mechanism of the failure of the grass cover.

431 The authors acknowledge that also other effects influence the results of the
432 existing models based on slope-parallel stresses. For instance, the turbulence in-
433tensities may vary along the slope leading to a change in (extreme) shear stresses,
434 which is also not taken into account by these models. However, we do not believe
435 that such an effect would explain the damage exactly at the location where the
436 overtopping waves impact the slope.

437 **5. Conclusions and Recommendations**

438 This paper presents a new method for predicting the onset of failure of grass
439 covered inner slopes of levees. The normal stresses exerted during wave overtop-
440 ping events have been shown to exceed the resistance. The cumulative effect of
441 normal stresses exerted by overtopping waves at the point of reattachment on the
442 landside slope has been shown to be indicative of the onset of failure of grass cov-
443 ers. Besides the critical load at which damage to the grass cover commences, the
444 method also predicts the location where damage will occur. The method has been
445 validated against two wave overtopping field tests performed in The Netherlands
446 and Belgium. However, the magnitude of the total excess momentum J_E at which
447 the grass cover is classified as 'failed' is not yet defined. It is recommended to
448 further study the critical magnitude of J_E and classify a critical load related to
449 condition of the grass cover. The new method was able to predict in 3 out of 4
450 cases the location where failure of the grass cover commenced. It is therefore rec-
451 ommended to further develop methods based on the peak transfer of momentum
452 with the levee whereby the effects of normal stresses at the point of reattachment
453 should be accounted for. In line with this further studies to the response of turf
454 layers to momentum exchange by wave overtopping is recommended to improve
455 the insights into the resistance of levees.

456 **6. Bibliography**

- 457 Bakker, J., Mom, R., Steendam, G., 2008. Factual report: Golfoverslagproeven
458 zeeuwse dijken. Tech. rep., INFRAM, Marknesse, The Netherlands.
- 459 Cantré, S., Olschewski, J., Saathoff, F., 2017. Full-scale flume experiments to ana-
460 lyze the surface erosion resistance of dike embankments made of dredged mate-
461 rials. *Journal of Waterway, Port, Coastal, Ocean Engineering* 143 (3).
- 462 Dean, R., Rosati, J., Walton, T., Edge, B., Jan 2010. Erosional equivalences of
463 levees: Steady and intermittent wave overtopping. *Ocean Engineering* 37, 104–
464 113.
- 465 EurOtop, 2007. Wave Overtopping of Sea Defences and Related Structures: As-
466 sessment Manual.
467 URL www.overtopping-manual.com
- 468 Führböter, A., 1966. Der druckschlag durch brecher auf deichböschungen. Ph.D.
469 thesis, Mitteilungen des Franzius-Instituts für Grund- und Wasserbau der Tech-
470 nischen Universität at Hannover.

- 471 Hai, T., Verhagen, H. J., 2014. Damage to grass covered slopes due to overtopping.
472 In: ICCE 2014: Proceedings of 34th International Conference on Coastal Engi-
473 neering, Seoul, Korea, 15-20 June 2014. Coastal Engineering Research Council.
- 474 Hewlett, H., 1985. Reinforcement of steep grassed waterways. Tech. Rep. 116,
475 CIRIA, London.
- 476 Hoffmans, G., 2014. Wti 2017 onderzoek en ontwikkeling landelijk toetsinstru-
477 mentarium, product 5.8 validatie erosiebestendigheid. Tech. rep., Deltares.
- 478 Hughes, S., May 2011. Adaptation of the levee erosional equivalence method for
479 the hurricane storm damage risk reduction system (hsdrrs). Tech. rep., US Army
480 Core of Engineers, Engineer Research and Development Center.
- 481 Hughes, S. A., Thornton, C., Van der Meer, J., Scholl, B., 2012. Improvements in
482 describing wave overtopping processes. In: Lynett, P., Smith, J. (Eds.), Coastal
483 Engineering 2012. No. 33.
- 484 Miedema, S., 2014. The Delft Sand, Clay & Rock Cutting Model. IOS Press.
- 485 Richwien, W., 2003. Die widerstandsfähigkeit von deichen beim wellenüberlauf
486 und die entwicklung von deichbrüchen-eine bestandsaufnahme.
- 487 Stanczak, G., 2007. Laboratory tests on the erosion of clay revetment of sea dike
488 with and without a grass cover induced by breaking wave impact. Tech. rep., TU
489 Braunschweig.
- 490 Stanczak, G., 2008. Breaching of sea dikes initiated from the seaside by breaking
491 wave impacts. Ph.D. thesis.
- 492 van Damme, M., Ponsioen, L., Herrero, M., Peeters, P., 2016. Comparing over-
493 flow and wave-overtopping induced breach initiation mechanisms in an embank-
494 ment breach experiment. In: E3S Web of Conferences. Vol. 7. EDP Sciences, p.
495 03004.
- 496 Van der Meer, J., van Hoven, A., Paulissen, A., Steendam, G., Verheij, H., Hoff-
497 mans, G., Kruse, G., 2012. Handreiking toetsen grasbekledingen op dijken t.b.v
498 het opstellen van het beheerdersoordeel (bo) in de verlengde derde toetsronde.
499 Tech. rep., Rijkswaterstaat, Ministerie van Infrastructuur en Milieu.
- 500 Van der Meer, W. J., 2002. Technisch rapport golfoploop en golfoverslag bij dijken,
501 (dutch). Tech. rep.
- 502 Van der Schrieck, G., 2006. Dredging Technology CT5300.

503 Whitehead, E., Bull, W., Schiele, M., 1976. A guide to the use of grass in hydraulic
504 engineering practice. Tech. rep.